An adaptive backstepping control to ensure the stability and robustness for boost power converter in DC microgrids

Zhang, Zehua; Song, Guiying; Zhou, Jiyao; Zhang, Xiaolu; Yang, Bowei; Liu, Chang; Guerrero, Josep M.

Published in:
Energy Reports

DOI (link to publication from Publisher):
10.1016/j.egyr.2022.02.024

Publication date:
2022

Document Version
Publisher's PDF, also known as Version of record

Available online at www.sciencedirect.com
ScienceDirect
Energy Reports 8 (2022) 1110–1124
www.elsevier.com/locate/egyr

2021 International Conference on New Energy and Power Engineering (ICNEPE 2021)
November 19 to 21, 2021, Sanya, China

An adaptive backstepping control to ensure the stability and robustness for boost power converter in DC microgrids

Zehua Zhang[a,b], Guiying Song[a,b,*], Jiyao Zhou[a,b], Xiaolu Zhang[c], Bowei Yang[a,b], Chang Liu[a,b], Josep M. Guerrero[d]

[a] *State Key Laboratory of Reliability and Intelligence of Electrical Equipment, School of Electrical Engineering, Hebei University of Technology, Tianjin 300130, China*

[b] *Key Laboratory of Electromagnetic Field and Electrical Apparatus Reliability of Hebei Province, Hebei University of Technology, Tianjin 300130, China*

[c] *North China Electric Power Research Institute Co., Ltd., Beijing 100045, China*

[d] *Center for Research on Microgrids (CROM), AAU Energy, Aalborg University, 9220 Aalborg East, Denmark*

Received 28 December 2021; accepted 3 February 2022
Available online 21 February 2022

Abstract

In recent years, the power electronic load infiltrates into the microgrid in the form of constant power, and its negative impedance characteristics threaten the stability of the system. To alleviate the instability caused by constant power loads (CPLs) and constant impedance loads (CILs) of the boost power converter in the DC microgrid, an adaptive backstepping control (BSC) method is designed. Firstly, based on the dynamic model of boost converter, an input voltage estimator is designed, which is introduced into backstepping control to improve the robustness to the change of input voltage. In addition, to improve the anti-interference performance of the system and ensure the static error free tracking of the output voltage, an extended nonlinear disturbance observer (ENDO) is used to compensate for the influence caused by mismatched disturbance and model uncertainty, the optimized BSC uses fewer initial parameters to ensure its operation. Finally, the large-signal stability of the proposed control is verified by using Lyapunov stability theory, which ensures the global trajectory tracking of the reference voltage and fast dynamic control. Through MATLAB simulation and hardware in the loop experiment (HIL), the proposed control is compared with BSC+NDO to verify the effectiveness and superiority of the proposed algorithm.

Peer-review under responsibility of the scientific committee of the 2021 International Conference on New Energy and Power Engineering, ICNEPE, 2021.

Keywords: DC microgrid; Boost converter; Constant power load; Backstepping control; Extended nonlinear disturbance observer; Large signal stability

* Corresponding author at: State Key Laboratory of Reliability and Intelligence of Electrical Equipment, School of Electrical Engineering, Hebei University of Technology, Tianjin 300130, China.
E-mail address: 202031404057@stu.hebut.edu.cn (G. Song).

https://doi.org/10.1016/j.egyr.2022.02.024

Peer-review under responsibility of the scientific committee of the 2021 International Conference on New Energy and Power Engineering, ICNEPE, 2021.

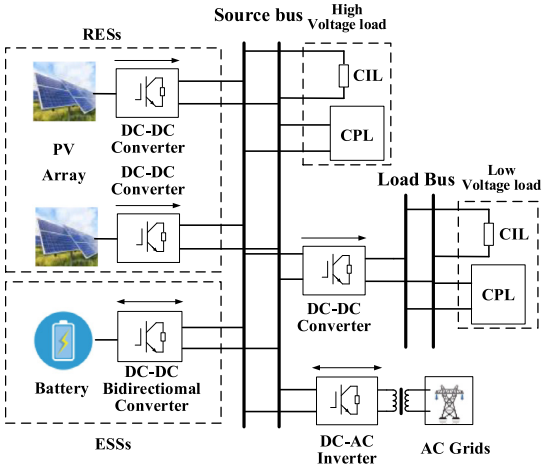

Fig. 1. Typical DC microgrid structure diagram.

1. Introduction

As an essential part of the intelligent power system in the future, the microgrid represents the development trend of renewable energy converging together with the power grid [1–4]. The microgrid is mainly divided into AC microgrid and DC microgrid. In recent years, the penetration rate of DC equipment such as a photovoltaic array, fuel cell, supercapacitor, motor driver, and notebook computer is increasing. DC microgrid effectively integrates power supply and load, reduces power conversion stage, improves transmission efficiency, and reduces system cost. Compared with the AC microgrid, the DC microgrid does not need to consider reactive power compensation, frequency problem, and skin effect. DC microgrid has natural advantages in improving system power supply reliability and power supply quality [5–9]. The typical DC microgrid structure diagram is shown in Fig. 1. The distributed generation and energy storage devices are connected to the high-voltage DC bus through a power electronic converter or to the low-voltage DC bus through secondary conversion to supply energy to the load side [10,11]. Microgrid loads are mainly divided into pure resistance load and constant power loads (CPLs). The former needs constant impedance to ensure its nominal operation, so it is also called constant impedance loads (CILs). The form of CPL in a microgrid is a strictly regulated power electronic converter. Its input voltage (current) decreases with the input current (voltage), thus consuming constant power, therefore, it is called a CPL. The consumption of constant power shows negative impedance characteristics at the input of a strictly regulated power electronic converter, reducing the system damping and destroying the stability of the feeder system and upstream converter. If there is no appropriate feedback control for regulation, the negative impedance characteristics will make the system unable to consume the transient energy of energy storage elements in the circuit. Then the energy in the energy storage element oscillates between inductance and capacitance, resulting in the limit cycle oscillation of the system [12–14]. This oscillation phenomenon will lead to the increase of switch stress, increased temperature, and decreased service period, the system cannot output stable voltage, which brings significant challenges to the operation and control of the system.

To eliminate the instability caused by CPLs, scholars have done much research. In literature [15,16] The passive damping method is designed. Although the system damping is increased and the stability is ensured by injecting passive components such as capacitance, inductance, and passive filter into the system, the added passive components consume energy and increase the circuit's cost and volume is not advocated in the practical system application. Therefore, to ensure the system's stable operation, an active damping method is designed in Refs. [17–19]. By injecting a virtual damping link into the control loop rather than adding damping to the circuit, the effect of series or parallel damping in the circuit is realized to improve the system damping and suppress the negative impedance characteristics of constant power load. However, passive and active damping is based on linear control in a small signal state, which can only provide accurate control performance in the small neighborhood of the equilibrium point. DC microgrid is a highly nonlinear system, linear control technology cannot maintain the global stability of

the system in an extended dynamic range. To overcome these defects, many algorithms based on nonlinear control are proposed. In Ref. [20], a backstepping sliding film controller is proposed to stabilize the large signal near the balance point and ensure the regulation of voltage when the load changes. However, the algorithm needs to detect the load current and input voltage, which increases the cost and complexity of the system, and the ideal control performance can be obtained only at a high switching frequency. However, the high switching frequency increases the switching loss, increases the electromagnetic interference to adjacent equipment, and has chattering. Ref. [21] proposed an adaptive passivity-based control (PBC). The algorithm combines passive control with a nonlinear disturbance observer (NDO). The primary control ensures the passivity of the system [22], and the nonlinear disturbance observer predicts the mismatched disturbance, which feedforward compensates it to the passive control to ensure good robustness and large-signal stability of the system. However, the design of the control requires many parameters, a complex design, and general dynamic performance. With the development of the microprocessor, model predictive control has gradually become a very advanced nonlinear control strategy [23]. Ref. [24] proposed an explicit model predictive control (eMPC) to ensure the stability of boost converter under constant power load. However, this control strategy requires the sensor to obtain the load current instead of the observer estimation, which will increase the cost of the system. It only considers a single constant power load, which is not suitable for industrial applications.

Backstepping control (BSC) is a recursive control algorithm based on Lyapunov. This method obtains the final control signal through the step backstepping algorithm of the system, it is one of the effective design tools to ensure that the system conforms to Lyapunov stability and output tracking [25]. However, due to the non-minimum phase characteristics of the boost converter in the DC microgrid, the backstepping algorithm cannot be controlled directly by voltage and current, but needs to convert the direct control into stored energy and input power through coordinate conversion to indirectly control the output voltage. In Ref. [26], adaptive backstepping control (ABSC) is designed. An online estimator is used to estimate the unknown parameters and introduced into BSC to ensure that the system output voltage has no deviation in case of sudden load change. However, this method does not consider the impact of constant power load on the system. In Ref. [27], for the boost converter with constant power load, BSC is combined with the Integral link. BSC ensures the system's stability, and the integration link eliminates the steady-state error of output voltage caused by inaccurate model and mismatched interference. However, the dynamic performance of the system is poor. As an effective technology for online estimation of nonlinear system disturbance, NDO can replace the traditional integral compensation disturbance and provide an effective solution for the compensation of inaccurate system models, uncertain parameters, and mismatched disturbance [28]. In Ref. [29], the backstepping control is combined with the NDO. BSC is used as the main controller to ensure that the system output converges to the nominal value. The NDO is used as the auxiliary controller to estimate the uncertain load changes, which feedforward compensation Channel to the main controller, so that the output voltage has no error. However, the complex nonlinear control involved requires more initial parameters, which is not conducive to practical applications, and when the load changes suddenly, the dynamic performance of the system is not outstanding.

In this paper, an improved backstepping control algorithm based on an extended nonlinear disturbance observer (ENDO) [30] is proposed to solve the instability problem of a boost converter with mixed load in a DC microgrid. The main controller optimizes the traditional backstepping control and designs an input voltage estimator into the backstepping control to run without input voltage and load information. The auxiliary controller uses an extended nonlinear disturbance observer to estimate the unmodeled and external disturbances of the system and feed forward to backstepping. The proposed composite nonlinear control can ensure fast and accurate output voltage nominal value tracking and large-signal stability under mixed load. The structure of this paper is as follows: the second section introduces the system modeling and problem introduction. The third section introduces the design of the compound nonlinear control strategy and the large-signal stability of the algorithm. The fourth and fifth sections give MATLAB simulation results and OPAL-RT based hardware-in-loop (HIL) experimental results, respectively. The sixth section gives the conclusion.

2. Mathematical model and problem description

As a strictly regulated power electronic converter, CPLs can be equivalent to a constant current source parallel negative impedance model, which guarantees both constant output power and negative impedance characteristics

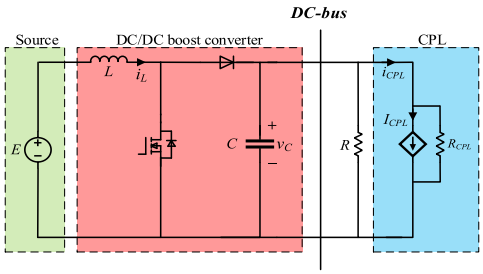

Fig. 2. DC–DC boost converter under mixed load.

[31].

$$\begin{cases} R_{CPL} = -\frac{v_{CPL}^2}{P_{CPL}} \\ I_{CPL} = \frac{2P_{CPL}}{v_{CPL}} \end{cases} \tag{1}$$

P_{CPL} is the power of constant power load, v_{CPL} represents the instantaneous value of input voltage, I_{CPL} represents the instantaneous value of constant current source current, and R_{CPL} is the negative impedance.

Fig. 2 is a cascaded system that simplifies the power supply and load in Fig. 1, which is composed of distributed power supply, boost converter, and hybrid load. E represents the distributed power supply for the boost converter, and the inductance and capacitance in the circuit are represented by L and C respectively. Lumped CILs is represented by R and lumped CPLs is represented by an equivalent model. The dynamic model can be represented as

$$\begin{cases} \frac{di_L}{dt} = \frac{E}{L} - \frac{v_C(1-u)}{L} \\ \frac{dv_C}{dt} = \frac{(1-u)i_L}{C} - \frac{v_C}{CR} - \frac{P_{CPL}}{Cv_C} \end{cases} \tag{2}$$

In formula (2), i_L and v_C represent inductance current and capacitance voltage, L, C and R are inductance, capacitance, and lumped CILs in the circuit, u is the duty cycle of the switch, and P_{CPL} is the power consumed by the lumped CPLs.

The control objective is to make the output voltage v_C track the voltage reference value v_{ref} under mixed loads. Because CILs have a positive damping effect, CPLs have a negative damping effect. Therefore, when they are cascaded in the system, CPLs dominate, and the system as a whole shows negative damping, resulting in system instability. Fig. 3 shows the root track of the system when CPLs dominate, it can be seen that the pole of the system is located on the right half axis of the root locus plane, and the system is in an unstable state.

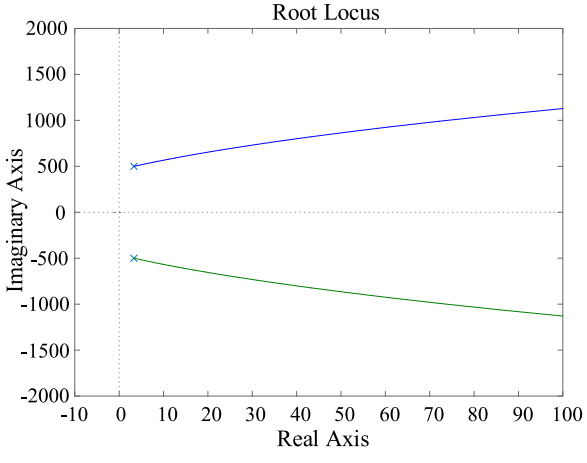

Fig. 3. CPLs dominant system root locus.

2.1. Coordinate transformation

The DC/DC boost converter in the DC microgrid is a highly nonlinear system and contains a non-minimum phase problem. If the inductive current is used to control the output voltage indirectly, it will lead to slow response and overshoot. Therefore, precise feedback linearization is used for coordinate conversion, and the output is redefined as system energy storage and input power to realize the minimum phase system [32].

The total energy stored in the system is expressed as

$$x_1 = \frac{1}{2}Li_L^2 + \frac{1}{2}Cv_C^2 \tag{3}$$

Take the time derivative of Eq. (3) as

$$\dot{x}_1 = Li_L\dot{i}_L + Cv_C\dot{v}_C = Ei_L - \frac{v_C^2}{R} - P_{CPL} \tag{4}$$

Based on Eq. (4), it can be assumed that the new state variable and unknown interference are defined as

$$x_2 = Ei_L \tag{5}$$

$$d_1 = -\frac{v_C^2}{R} - P_{CPL} \tag{6}$$

Combined with (2) and (6), the total power at the load side of the DC/DC boost converter can be set as

$$P_{ref} = \frac{v_C^2}{R} + P_{CPL} = -d_1 \tag{7}$$

The time derivative of Eq. (5) can be obtained

$$\dot{x}_2 = \frac{E^2}{L} - \frac{Ev_C}{L}(1-u) + d_2 \tag{8}$$

The system of Eq. (2) can be reconverted to the canonical form

$$\begin{cases} \dot{x}_1 = x_2 + d_1 \\ \dot{x}_2 = V + d_2 \end{cases} \tag{9}$$

The above formula V is the intermediate control rate, and d_2 is the unmodeled and parameter uncertainty interference. According to the above formula (8) and (9), the final control rate of the initial system (2) is

$$u = 1 - \frac{E^2 - VL}{Ev_C} \tag{10}$$

3. The construction of the proposed controller

In this section, in order to stabilize the boost converter with mixed loads, make it robust, and output voltage zero error, an adaptive backstepping control is designed. The control is divided into three parts: the design of the distributed power supply voltage estimator, the extended NDO, and the design of the backstepping controller. The voltage estimator estimates the input voltage and expands NDO to predict various mismatch disturbances and unmodeled disturbances to compensate for the backstepping controller to generate a PWM pulse signal for driving the MOSFET of the boost converter. Finally, the Lyapunov function is used to verify the global stability of the controller [33].

3.1. Voltage estimator design

The voltage of distributed power supply is usually unknown and time-varying. In order to ensure the stability of the designed controller and reduce the number of sensors, an estimator is designed to estimate the power supply voltage. The error is defined as

$$\widetilde{E} = \hat{E} - E \tag{11}$$

In Eq. (11), $\widetilde{E}$ represents the estimated error of the power supply voltage, $\hat{E}$ represents the estimated value of the power supply voltage, and the voltage estimator is designed as

$$\hat{E} = E_I + \lambda x \tag{12}$$

In the formula (12), $\lambda > 0$, E_I represents the auxiliary variable, x represents the inductor current in formula (2), and the time derivative of the formula (11) can be obtained

$$\dot{\widetilde{E}} = \dot{E}_I + \lambda \dot{x} = \dot{E}_I + \lambda \left(\frac{\hat{E} - \widetilde{E}}{L} - \frac{(1-u)\, v_C}{L} \right) \tag{13}$$

To ensure that the designed controller satisfies the stability condition of the Lyapunov function, the design takes the auxiliary variable $\dot{E}_I$ as

$$\dot{E}_I = -\lambda \left(\frac{\hat{E}}{L} - \frac{(1-u)\, v_C}{L} \right) \tag{14}$$

Substituting formula (14) into formula (13) can be simplified to get

$$\dot{\widetilde{E}} = -\frac{\lambda}{L} \widetilde{E} \tag{15}$$

According to formula (15). Selecting the appropriate coefficient λ can ensure that the designed voltage estimator satisfies the Lyapunov indirect stability condition and is asymptotically stable globally.

3.2. Design of extended nonlinear disturbance observer

The assumed disturbance are caused by the fluctuation of the mixed load side, the uncertainty of the circuit parameters and the interference of the system for modeling, so reasonable assumptions can be made [34].

$$\left| \frac{\mathrm{d}^j d_i(t)}{\mathrm{d}t^j} \right| \leq \delta,\ j = 1, 2 \ldots, n \tag{16}$$

The extended nonlinear disturbance observer used in this paper is mainly used to estimate the disturbance and compensate it to reach the output voltage tracking rated voltage in the backstepping controller. Because the extended nonlinear disturbance observer also estimates the time derivative of the disturbance, it has a better dynamic response than NDO.

Firstly, the uncertainty d_1 is estimated

$$\begin{cases} \hat{d}_1 = P_{11} + l_{11} x_1 \\ \dot{P}_{11} = -l_{11} \left(x_2 + \hat{d}_1 \right) + \widehat{\dot{d}}_1 \\ \widehat{\dot{d}}_1 = P_{12} + l_{12} x_1 \\ \dot{P}_{12} = -l_{12} \left(x_2 + \hat{d}_1 \right) \end{cases} \tag{17}$$

Similarly, the extended NDO is used to estimate the unmodeled and parameter uncertainty interference d_2

$$\begin{cases} \hat{d}_2 = P_{21} + l_{21} x_2 \\ \dot{P}_{21} = -l_{21} \left(V + \hat{d}_2 \right) + \widehat{\dot{d}}_2 \\ \widehat{\dot{d}}_2 = P_{22} + l_{22} x_2 \\ \dot{P}_{22} = -l_{22} \left(V + \hat{d}_2 \right) \end{cases} \tag{18}$$

In Eqs. (17) and (18), P_{i1}, P_{i2} $(i = 1, 2)$ are auxiliary variables in the extended NDO, l_{i1}, l_{i2} $(i = 1, 2)$ are the extended NDO gains, and $\hat{d}_i$, $\widehat{\dot{d}}_i (i = 1, 2)$ are the interference estimated value and the interference estimated value Derivative.

According to the above formula, the estimated error $\widetilde{d}_1, \widetilde{d}_2$ can be defined as

$$\widetilde{e}_i = \left[\widetilde{d}_i, \widetilde{\dot{d}}_i \right]^T (i = 1, 2) \tag{19}$$

$$\widetilde{d}_i = d_i - \hat{d}_i \ (i = 1, 2) \tag{20}$$

From Eqs. (9), (17), (18) and (20), we can get

$$\dot{\hat{d}}_i = l_{i1}\widetilde{d}_i + \widehat{\dot{d}}_i \tag{21}$$

$$\dot{\widetilde{d}}_i = -l_{i1}\widetilde{d}_i + \widetilde{\dot{d}}_i \ (i = 1, 2) \tag{22}$$

Similarly, it can be derived

$$\dot{\widetilde{d}}_i = -l_{i2}\widetilde{d}_i + \ddot{d}_i \tag{23}$$

The observer dynamic error expression is

$$\dot{\widetilde{e}}_i = G_i\widetilde{e}_i + H_i\ddot{d}_i (i = 1, 2) \tag{24}$$

$$G_i = \begin{bmatrix} -l_{i1} & 0 \\ -l_{i2} & 0 \end{bmatrix}, H_i = \begin{bmatrix} 0 \\ 1 \end{bmatrix} \tag{25}$$

According to the assumption that the perturbation is bounded and known as a normal number, $H_i\ddot{d}_i$ can be ignored. Eq. (24) can satisfy the indirect conditions of Lyapunov stability by selecting an appropriate gain to ensure the global stability of the designed extended NDO.

3.3. Design of backstepping controller

The backstepping controller based on extended NDO and voltage estimator designed in this section is divided into two parts:

i. Solving the nominal value x_2^*

The goal of backstepping control is to make the new state variable x_1, x_2 gradually track to the nominal value x_1^*, x_2^* after coordinate conversion, so the state variable error is expressed as

$$\begin{cases} z_1 = x_1 - x_1^* \\ z_2 = x_2 - x_2^* \end{cases} \tag{26}$$

Derived from (3) and (7), the nominal value x_1^* can be obtained

$$x_1^* = \frac{1}{2}L\left(\frac{P_{ref}}{\hat{E}}\right)^2 + \frac{1}{2}Cv_{ref}^2 = \frac{1}{2}\frac{L}{\hat{E}^2}(-d_1)^2 + \frac{1}{2}Cv_{ref}^2 \tag{27}$$

Derivation of Eq. (26) z_1 can be obtained

$$\dot{z}_1 = \dot{x}_1 - \dot{x}_1^* = z_2 + x_2^* + d_1 \tag{28}$$

Define the Lyapunov function V_1

$$V_1 = \frac{1}{2}z_1^2 + \frac{1}{2}\widetilde{d}_1^2 \tag{29}$$

$$\dot{V}_1 = z_1\left(z_2 + x_2^* + \hat{d}_1\right) + z_1\widetilde{d}_1 - l_{11}\widetilde{d}_1^2 + \widetilde{d}_1\dot{\widetilde{d}}_1 \tag{30}$$

To make V_1 satisfy the Lyapunov stability condition, the nominal value x_2^* is designed as

$$x_2^* = -k_1z_1 - \hat{d}_1 \ (k_1 > 0) \tag{31}$$

Substituting formulas (20), (21) and (31) into (30) and simplifies as

$$\dot{V}_1 = -k_1z_1^2 + z_1z_2 + z_1\widetilde{d}_1 - l_{11}\widetilde{d}_1^2 + \widetilde{d}_1\dot{\widetilde{d}}_1 \tag{32}$$

At this time, it can be seen from Eq. (32) that the system does not satisfy the Lyapunov negative definite condition, and proceed to the next step.

ii. Solving the virtual control rate V

Taking the time derivative of z_2 in Eq. (26), we can get

$$\dot{z}_2 = \dot{x}_2 - \dot{x}_2^* = V + d_2 + k_1\dot{z}_1 + \dot{\hat{d}}_1 \tag{33}$$

Select Lyapunov function V_2

$$V_2 = V_1 + \frac{1}{2}z_2^2 + \frac{1}{2}\tilde{d}_2^2 \tag{34}$$

Take the derivative of V_2 and combine (21), (31) and (33) to simplify

$$\dot{V}_2 = \dot{V}_1 + z_2\left[V + \hat{d}_2 + k_1\left(-k_1z_1 + \tilde{d}_1 + z_2\right) + l_{11}\tilde{d}_1 + \dot{\hat{d}}_1\right] + z_2\tilde{d}_2 + \tilde{d}_2\dot{\tilde{d}}_2 \tag{35}$$

To make (35) satisfy the Lyapunov negative definite condition, the virtual control rate V is designed as

$$V = -k_2z_2 - \hat{d}_2\,(k_2 > 0) \tag{36}$$

In summary, the schematic diagram of the proposed controller is shown in Fig. 4.

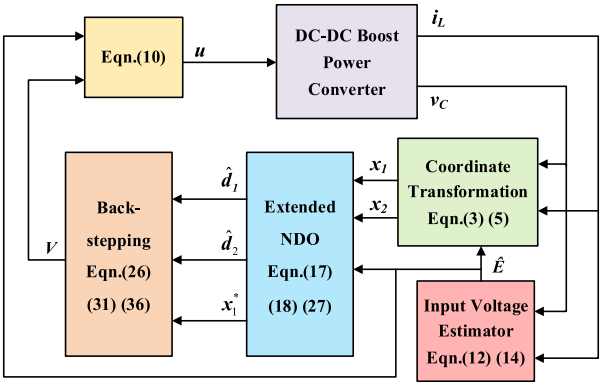

Fig. 4. Diagram of the proposed control method.

3.4. Proposal controller stability analysis

Through formulas (21), (22), (32), (35), (35) and (36) can be simplified to

$$\dot{V}_2 = -k_1z_1^2 - k_2z_2^2 + \left(1 - k_1^2\right)z_1z_2 + z_1\tilde{d}_1 - l_{11}\tilde{d}_1^2 + \tilde{d}_1\dot{\tilde{d}}_1 + k_1z_2\tilde{d}_1 + k_1z_2^2 + l_{11}\tilde{d}_1z_2 + \dot{\hat{d}}_1z_2 + z_2\tilde{d}_2 - l_{21}\tilde{d}_2^2 + \tilde{d}_2\dot{\tilde{d}}_2 \tag{37}$$

Combining the principle of inequality $2ab \le a^2 + b^2$, the simplified formula (37) can be obtained

$$\begin{aligned}\dot{V}_2 \le {} & -\frac{1}{2}\left(k_1^2 + 2k_1 - 2\right)z_1^2 - \frac{1}{2}\left[2k_2 - \left(1 - k_1^2\right) - 3k_1 - l_{11} - 2\right]z_2^2 - \frac{1}{2}\left(l_{11} - k_1 - 2\right)\tilde{d}_1^2 \\ & - \left(l_{21} - 1\right)\tilde{d}_2^2 + \frac{1}{2}\dot{\tilde{d}}_1^2 + \frac{1}{2}\dot{\tilde{d}}_2^2 + \frac{1}{2}\dot{\hat{d}}_1^2\end{aligned} \tag{38}$$

To make the constructed Lyapunov function a negative definite, the system is guaranteed to satisfy the Lyapunov stability condition. The parameters are selected as

$$\begin{cases} k_1^2 + 2k_1 - 2 > 0 \\ 2k_2 - \left(1 - k_1^2\right) - 3k_1 - l_{11} - 2 > 0 \\ l_{11} - k_1 - 2 > 0 \\ l_{21} - 1 > 0 \end{cases} \Rightarrow \begin{array}{c} k_1 > -1 + \sqrt{3} \\ k_2 > \frac{1 - k_1^2 + 3k_1 + l_{11} + 2}{2} \\ l_{11} > k_1 + 2 \\ l_{21} > 1 \end{array} \tag{39}$$

When the parameter selection in the controller satisfies the value of Eq. (39), and the independent variable of the designed Lyapunov function approaches infinity, the value of the Lyapunov function also approaches infinity, the closed-loop system is globally stable, which means that the system can complete the gradual tracking of the new

Table 1. System parameter.

Symbol	Description	Values
E	Input voltage	375 V
L	Boost inductor	1 mH
C	Boost capacitor	2.2 mF
R	Nominal resistive load	50 Ω
P_{CPL}	Nominal power of CPL	15 kW
f_s	Switching frequency	20 kHz
V_{ref}	Output voltage reference	750 V

Table 2. Controller parameters.

Algorithm	Observer gain	Controller gain	Voltage estimation gain
BSC+NDO	$l_1 = 300,\ l_2 = 200$	$k_1 = 800,\ k_2 = 4000$	–
Proposed control	$l_{11} = 1540,\ l_{12} = 1000$ $l_{21} = 800,\ l_{22} = 300$	$k_1 = 800,\ k_2 = 4000$	25

state variables, so the DC bus voltage can reach the reference value, and with the help of the observer, the system can keep the output steady-state without error under various uncertain disturbances.

4. Simulation results and discussions

The system model was built through MATLAB/Simulink, and the algorithm's large-signal stability and anti-interference robustness was verified by simulation. The system parameters in Fig. 2 are given in Table 1, and Table 2 shows the parameters of the proposed control algorithm and the BSC+NDO [25] control algorithm for comparison. Then, the simulation results under different working conditions are compared and discussed.

4.1. Input voltage interference test

Fig. 5 shows the dynamic performance of the proposed control (in red) and BSC+NDO (in blue) during input voltage changes. The change in input voltage and the predicted value of the voltage estimator are shown in the first graph in Fig. 5. The input voltage jumps from 375 V to 325 V at 0.08 s, and then from 325 V to 425 V

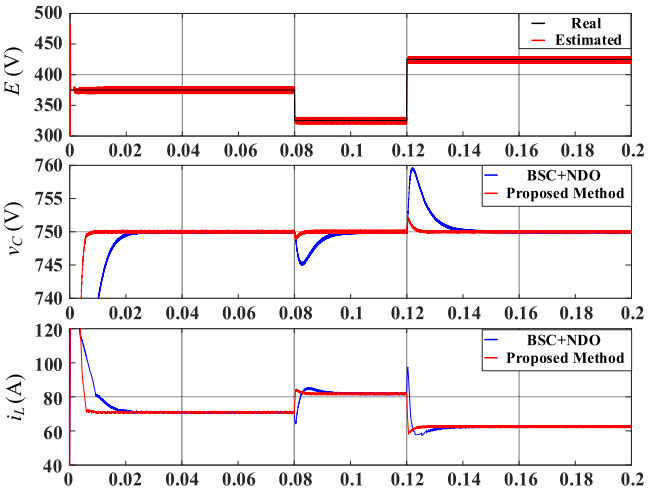

Fig. 5. Voltage and current waveforms with input voltage variation. (For interpretation of the references to color in this figure legend, the reader is referred to the web version of this article.)

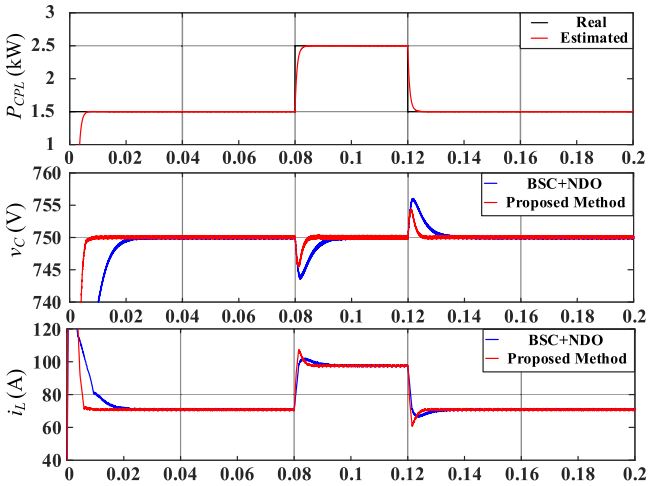

Fig. 6. Voltage and current waveforms with CPL power variation. (For interpretation of the references to color in this figure legend, the reader is referred to the web version of this article.)

after 0.04 s. It can be seen that BSC+NDO will produce a higher instantaneous voltage drop when the input voltage changes suddenly, although it can eliminate the steady-state error caused by the input voltage change within 25 ms. However, the control method proposed in this paper can be restored to the nominal value in only 4 ms, the instantaneous voltage drop is minimal. The inductor current stabilizes faster at startup, and when the input voltage changes suddenly, the inductor current has a small overshoot and a short recovery time. The results show that the DC microgrid exhibits excellent robustness when the proposed control responds to the intermittent voltage step changes of distributed power generation.

4.2. CPL disturbance test

Fig. 6 shows the dynamic performance of the proposed control (in red) and BSC+NDO (in blue) during CPL changes. The actual change of CPL and the estimated value of disturbance are shown in the first graph in Fig. 6. The CPL jumped from 15 kW to 25 kW at 0.08 s and then recovered from 25 kW to 15 kW after 0.04 s. It can be seen from the figure that BSC+NDO will produce an instantaneous voltage drop of 7 V after the CPL mutation, although it can eliminate the steady-state error caused by the CPL change within 18 ms. However, the control proposed in this article only 7 ms to recover to the nominal value, the instantaneous voltage drop is only 4 V, and the inductive current reaches stability faster. The results show that when the proposed control responds to the step change of CPL, the output of the DC microgrid system is stable without error and has outstanding dynamic performance.

4.3. CIL disturbance test

Fig. 7 shows the dynamic performance of the proposed control (in red) and BSC+NDO (in blue) when CIL changes. CIL changes from 50 Ω to 100 Ω at 0.08 s, and after 0.04 s, it recovers from 100 Ω to 50 Ω. As can be seen from the figure, after the CIL mutation of BSC+NDO, the DC bus voltage will have an instantaneous change of 3 V, although it can be within 17 ms. Eliminate the steady-state error generated when the CIL changes. However, the proposed control in this article only takes 7 ms to restore the DC bus voltage to the nominal value, and the instantaneous voltage change is only 2 V. The results show that when the proposed control responds to the step change of CIL, the output of the DC microgrid system is stable without error and has outstanding dynamic performance.

4.4. Capacitance uncertainty test

The control proposed in this paper is robust to the uncertainty of the system parameters. When there is an error between the system capacitance parameters and the parameters in the controller, it will not affect the stability of

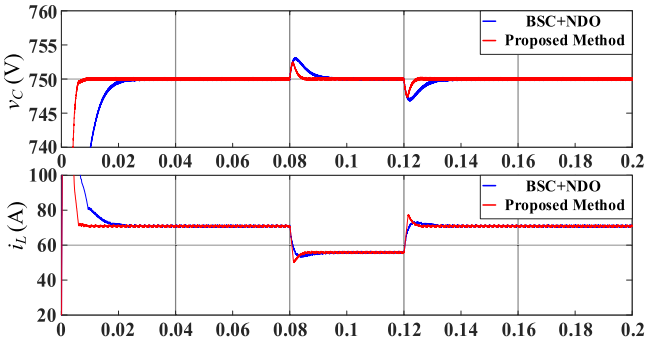

Fig. 7. Voltage and current waveforms with resistance variation. (For interpretation of the references to color in this figure legend, the reader is referred to the web version of this article.)

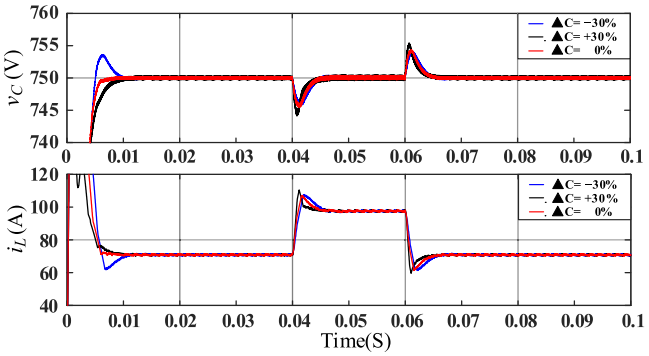

Fig. 8. Voltage and current waveforms with capacitance uncertainty.

the boost converter with mixed loads. Fig. 8 shows the dynamic performance of the DC bus voltage and inductor current after a sudden change in the CPL load occurs during the period when the capacitance of the output side of the system is uncertain. The uncertainty of the capacitance is 70% and 130% of the nominal value. The results show that a lower capacitance uncertainty will cause a slight start-up overshoot, and a higher capacitance uncertainty will cause a larger instantaneous voltage drop, but both can make the system runs stably, and the DC bus voltage has no deviation. The results show that the proposed control is robust to the uncertainty of the system parameters and can be better adapted to industrial applications in a variety of situations.

5. Hardware-in-loop experimental results

In this section, to further verify the effectiveness of the proposed control, a hardware-in-loop (HIL) experimental platform based on OPAL-RT is built. This platform allows the MATLAB/Simulink hardware model to be put into the OPAL-RT real-time simulator. he digital processing system TMS320F28379 (DSP) receives the signals (i_L, v_C) output by the OPAL-RT real-time simulator, to successively execute the input voltage estimator, backstepping control and extended NDO. Finally, the PWM signal is output and sent to the digital input port of OPAL-RT as the gate signal of MOSFET in the boost converter. Oscilloscope is used to observe the control effect. The experimental flow chart is shown in Fig. 9.

In order to further verify the effectiveness of the proposed control, a HIL experiment was carried out, as shown in Fig. 10. During this experiment, the load maintain CPL at 15 kW, CIL at 50 Ω, and the input voltage interference settings were the same as in Fig. 5. It can be observed that BSC+NDO (blue, CH2) can guarantee to track the reference voltage during the input voltage change period, but its voltage instantaneous change range is large, and the recovery time is also long. However, for the proposed control in this article (red, CH1), the instantaneous change and recovery time of the DC bus voltage is only 1/5 and 1/6 of BSC+NDO. Compared with BSC+NDO (blue,

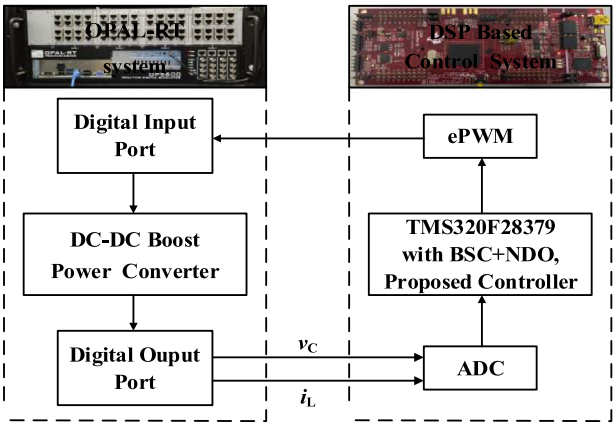

Fig. 9. Block diagram represents the HIL experiment platform.

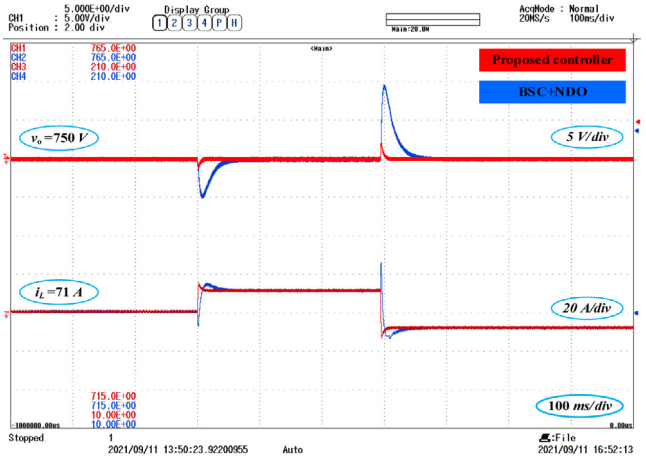

Fig. 10. Voltage and current waveforms with input voltage variation compared with BSC+NDO in HIL. (For interpretation of the references to color in this figure legend, the reader is referred to the web version of this article.)

CH4), the inductance current of this article is recommended to control (red, CH2) when the input voltage changes suddenly, there is no obvious overshoot, and its dynamic performance is better.

To further verify the effectiveness under the sudden change of CPL power, a HIL experiment was carried out, as shown in Fig. 11. In this experiment, the input voltage and CIL 50 Ω remain unchanged, and the sudden change of CPL power generation remains the same as in Fig. 6. It can be observed that the recovery time required for the proposed control (red, CH1, CH3) to reach a steady-state is only 1/3 of BSC+NDO (blue, CH2, CH4). For the overshoot of the DC bus voltage, The voltage overshoot of BSC+NDO is 7 V, and the voltage overshoot of proposed control is only 4 V. The experimental results show that the proposed control can show excellent dynamic performance after a sudden change in CPL.

Fig. 12 shows the HIL experimental verification of the simulation results in Fig. 7. In this experiment, the input voltage remains the same as the 15 kW of CPL, and the mutation generated by CIL remains the same as in Fig. 7. It can be observed that the recovery time required for the proposed control (red, CH1, CH3) to reach a steady-state is only 1/3 of BSC+NDO (blue, CH2, CH4). For the overshoot of the DC bus voltage, The voltage overshoot of BSC+NDO is 3 V, and the voltage overshoot of proposed control is only 2 V. The experimental results show that the proposed control can show excellent dynamic performance after a sudden change in CIL.

To verify the effectiveness of the proposed control under the uncertainty of the system parameters, a HIL experiment was carried out, as shown in Fig. 13. In this experiment, assuming that the capacitance uncertainty

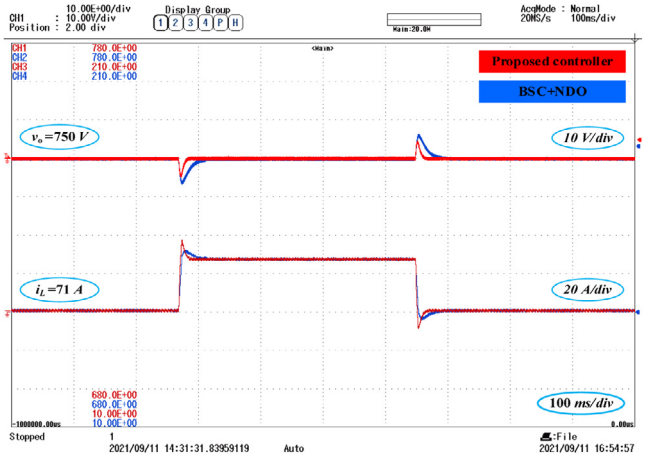

Fig. 11. Voltage and current waveforms with CPL variation compared with BSC+NDO in HIL. (For interpretation of the references to color in this figure legend, the reader is referred to the web version of this article.)

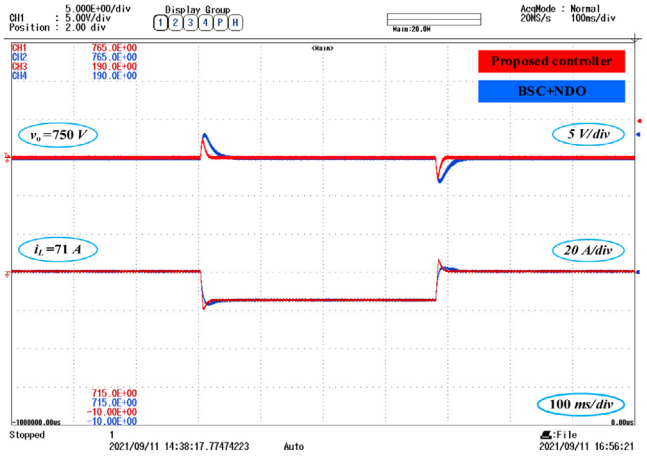

Fig. 12. Voltage and current waveforms with resistance variation compared with BSC+NDO in HIL. (For interpretation of the references to color in this figure legend, the reader is referred to the web version of this article.)

is 30% lower (blue) and 30% higher (green) than the nominal value respectively, the sudden change in CPL power remains the same as in Fig. 6. It can be observed that when the proposed control deviates from the nominal value with different capacitance values, the DC bus voltage can still be steady without error. Therefore, it is concluded that the proposed control is robust to model uncertainty. The experimental results show that the proposed control is robust to the uncertainty of model parameters and has a good application prospect in industrial applications where the system parameters cannot be accurately measured.

6. Conclusion

In this paper, because of the system instability caused by the mixed load of the boost power converter inside the DC microgrid, adaptive backstepping control is proposed to ensure the stability of the large-signal of the system. Under the premise that the required system initial parameters are few, the designed voltage estimator and ENDO eliminate the steady-state error of the DC bus voltage caused by mismatch interference, input voltage change, and model uncertainty, and dynamic performance is good, the controller parameters are designed by using Lyapunov stability condition to ensure the global stability of the system. BSC+NDO is compared with the proposed control through MATLAB/Simulink simulation and HIL experiments. Based on the above results, it can be found that the

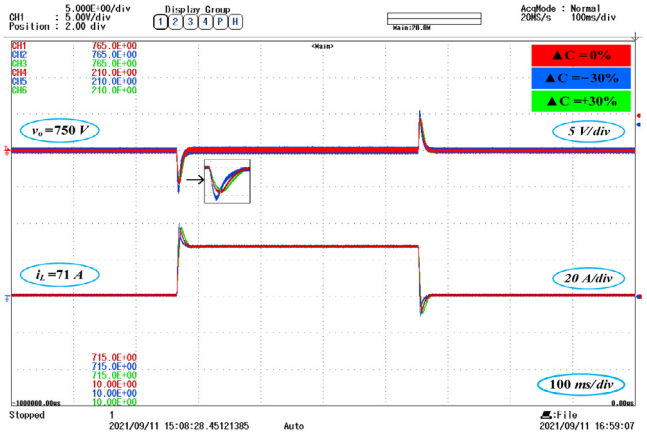

Fig. 13. Voltage and current waveforms with the uncertain capacitance in HIL. (For interpretation of the references to color in this figure legend, the reader is referred to the web version of this article.)

proposed control has good performance in startup, settling time, and overshoot, so it has better robustness and dynamic. This research is suitable for the industrial application of DC microgrid to ensure stable operation of DC microgrid under mixed load and excellent performance.

Declaration of competing interest

The authors declare that they have no known competing financial interests or personal relationships that could have appeared to influence the work reported in this paper.

References

[1] Parhizi Sina, Lotfi Hossein, Khodaei Amin, Bahramirad Shay. State of the art in research on microgrids: A review. IEEE Access 2015;3:890–925.
[2] Olivares Daniel E, Mehrizi-Sani Ali, Etemadi Amir H, Canizares Claudio A, Iravani Reza, Kazerani Mehrdad, et al. Trends in microgrid control. IEEE Trans Smart Grid 2014;5(4):1905–19.
[3] Meng Lexuan, Shafiee Qobad, Trecate Giancarlo Ferrari, Karimi Houshang, Fulwani Deepak, Lu Xiaonan, et al. Review on control of DC microgrids and multiple microgrid clusters. IEEE J Emerg Sel Top Power Electron 2017;5(3):928–48.
[4] Peyghami Saeed, Palensky Peter, Blaabjerg Frede. An overview on the reliability of modern power electronic based power systems. IEEE Open J Power Electron 2020;1(2020):34–50.
[5] Kumar Dinesh, Zare Firuz, Ghosh Arindam. DC microgrid technology: System architectures, AC grid interfaces, grounding schemes, power quality, communication networks, applications and standardizations aspects. IEEE Access 2017;5:12230–56.
[6] Dragicevic Tomislav, Lu Xiaonan, Vasquez Juan, Guerrero Josep. DC microgrids–Part I: A review of control strategies and stabilization techniques. IEEE Trans Power Electron 2016;31(7):4876–91.
[7] Dragicevic Tomislav, Lu Xiaonan, Vasquez Juan C, Guerrero Josep M. DC microgrids—Part II: A review of power architectures, applications, and standardization issues. IEEE Trans Power Electron 2016;31(5):3528–49.
[8] Espina Enrique, Llanos Jacqueline, Burgos-Mellado Claudio, Cardenas-Dobson Roberto, Martinez-Gomez Manuel, Saez Doris. Distributed control strategies for microgrids: An overview. IEEE Access 2020;193412-193448.
[9] Yousefizadeh Shirin, Bendtsen Jan Dimon, Vafamand Navid, Khooban Mohammad Hassan, Blaabjerg Frede, Dragicevic Tomislav. Tracking control for a DC microgrid feeding uncertain loads in more electric aircraft: Adaptive backstepping approach. IEEE Trans Ind Electron 2019;66(7):5644–52.
[10] Frances Airan, Asensi Rafael, Garcia Oscar, Prieto Roberto, Uceda Javier. Modeling electronic power converters in smart DC microgrids—An overview. IEEE Trans Smart Grid 2018;9(6):6274–87.
[11] Naderi M, Bahramara S, Khayat Y, Bevrani H. Optimal planning in a developing industrial microgrid with sensitive loads. Energy Rep 2017;3:124–34.
[12] Singh Suresh, Gautam Aditya R, Fulwani Deepak. Constant power loads and their effects in DC distributed power systems: A review. Renew Sustain Energy Rev 2017;72:407–21.
[13] Kwasinski Alexis, Onwuchekwa Chimaobi N. Dynamic behavior and stabilization of DC microgrids with instantaneous constant-power loads. IEEE Trans Power Electron 2011;26(3):822–34.
[14] Emadi Ali, Khaligh Alireza, Rivetta Claudio H, Williamson Geoffrey A. Constant power loads and negative impedance instability in automotive systems: Definition, modeling, stability, and control of power electronic converters and motor drives. IEEE Trans Veh Technol 2006;55(4):1112–25.

[15] Mayo-Maldonado JC, Rapisarda P. A systematic approach to constant power load stabilization by passive damping. In: IEEE 54th annual conference on decision and control. 2015. p. 1346–51.
[16] Cespedes Mauricio, Xing Lei, Sun Jian. Constant-power load system stabilization by passive damping. IEEE Trans Power Electron 2011;26(7):1832–6.
[17] Liu Xinyun, Forsyth Andrew J, Cross Andrew M. Negative input-resistance compensator for a constant power load. IEEE Trans Ind Electron 2007;54(6):3188–96.
[18] Wu Mingfei, Lu Dylan Dah-Chuan. A novel stabilization method of LC input filter with constant power loads without load performance compromise in DC microgrids. IEEE Trans Ind Electron 2015;62(7):4552–62.
[19] Xiaonan Lu, Sun Kai, Guerrero Josep M, Vasquez Juan C, Huang Lipei, Wang Jianhui. Stability enhancement based on virtual impedance for DC microgrids with constant power loads. IEEE Trans Smart Grid 2015;6(6):2770–83.
[20] Wu Jiarong, Lu Yimin. Adaptive backstepping sliding mode control for boost converter with constant power load. IEEE Access 2019;7:50797–807.
[21] Hassan Mustafa Alrayah, He Yigang. Constant power load stabilization in DC microgrid systems using passivity-based control with nonlinear disturbance observer. IEEE Access 2020;8:92393–406.
[22] Riccobono Antonino, Santi Enrico. Comprehensive review of stability criteria for DC power distribution systems. IEEE Trans Ind Appl 2014;50(5):3525–35.
[23] Vazquez Sergio, Rodriguez Jose, Rivera Marco, Franquelo Leopoldo G, Norambuena Margarita. Model predictive control for power converters and drives: Advances and trends. IEEE Trans Ind Electron 2017;64(2):935–47.
[24] Andres-Martinez Oswaldo, Flores-Tlacuahuac Antonio, Ruiz-Martinez Omar F, Mayo-Maldonado Jonathan C. Nonlinear model predictive stabilization of DC–DC boost converters with constant power loads. IEEE J Emerg Sel Top Power Electron 2021;9(1):822–30.
[25] Ashabani Seyed Mahdi, Mohamed Yasser Abdel-Rady I. A flexible control strategy for grid-connected and islanded microgrids with enhanced stability using nonlinear microgrid stabilizer. IEEE Trans Smart Grid 2012;3(3):1291–301.
[26] Boutebba Okba, Semcheddine Samia, Krim Fateh, Talbi Billel. 2019. Adaptive nonlinear controller design for DC-DC buck converter via backstepping methodology. In: IEEE 2019 international conference on advanced electrical engineering. 2019. p. 1–7.
[27] Khan Muhammad Saud, Ahmad Iftikhar, Zain Ul Abideen Farrukh. Output voltage regulation of FC-UC based hybrid electric vehicle using integral backstepping control. IEEE Access 2019;7:65693–702.
[28] Chen Wen-Hua, Yang Jun, Guo Lei, Li Shihua. Disturbance-observer-based control and related methods—An overview. IEEE Trans Ind Electron 2016;63(2):1083–95.
[29] Xu Qianwen, Zhang Chuanlin, Wen Changyun, Wang Peng. A novel composite nonlinear controller for stabilization of constant power load in DC microgrid. IEEE Trans Smart Grid 2019;10(1):752–61.
[30] Ginoya Divyesh, Shendge PD, Phadke SB. Sliding mode control for mismatched uncertain systems using an extended disturbance observer. IEEE Trans Ind Electron 2014;61(4):1983–92.
[31] Tahim Andre Pires Nobrega, Pagano Daniel J, Lenz Eduardo, Stramosk Vinicius. Modeling and stability analysis of islanded DC microgrids under droop control. IEEE Trans Power Electron 2015;30(8):4597–607.
[32] Arora Sameer, Balsara Poras, Bhatia Dinesh. Input–output linearization of a boost converter with mixed load (constant voltage load and constant power load). IEEE Trans Power Electron 2019;34(1):815–25.
[33] Shaker Hamid Reza. Lyapunov stability for continuous-time 2D nonlinear systems. In: IEEE 52nd IEEE conference on decision and control. 2013. p. 4586–9.
[34] Su Jinya, Chen Wen-Hua, Li Baibing. High order disturbance observer design for linear and nonlinear systems. In: 2015 IEEE international conference on information and automation. p. 1893–8.